ICAS 2021 SHANGHAI
International Council of the Aeronautical Sciences
32nd Congress of the International Council of the Aeronautical Sciences
September 6-10, 2021
Pudong Shangri-La, Shanghai, China

HELICOPTER FLIGHT DYNAMICS MODELLING WITH FREE-WAKE METHOD EMBEDDED FOR ROTOR ICING ANALYSES

Guozhi Li [1], Guanglin Zhang [2] & Shiyong Chu [2]

1 Chinese Aeronautical Establishment

2 Aviation Industry Development Research Center of China

Abstract

A free-wake method embedded in a helicopter flight dynamics model for rotor icing analyses is presented. The rotor wake geometries of UH-60A helicopter at different flight velocities are numerically computed and demonstrated. Effects of icing on the rotor wake are then analyzed. The results indicate that both the sunk trend of the wake due to ice accretion and the variation on ice shape accreted on the surface of the blades might lead to the rotor aerodynamics degradation for example the decrease in the lift coefficient and the increase in the drag coefficient.

Keywords: Helicopter; Rotor wake; Flight dynamics; Aerodynamics; Ice accretion

1. Introduction

Rotor blade ice accretion, which mainly affects the rotor wake geometry and its aerodynamics characteristics, degrades the flight performance and flying qualities, and even threats the helicopter flight safety, is a great hazardous factor that requires attention on helicopter design. Understanding sensitivity of ice accretion and aerodynamics performance as well as flight dynamics characteristics degradation is essential in helicopter certification program to ensure safe flight in icing conditions. Since the last 40 years, some researchers, having experience in experimental and theoretical studies on airplane and propeller system in icing conditions, investigated the potentially hazardous effects of ice accretion on rotor blades [1, 2]. Over the past decade, studies on the flight dynamics characteristics of CH-47B and UH-60A helicopter in well-known meteorological icing conditions have been conducted sufficiently by developing numerical methods and analyses models [3, 4]. Cao has a continuous in-depth study of the icing problem [5, 6]. However, works on effects of inflight icing on rotor wake, which have the key aerodynamic interference effects on the helicopter fuselage, horizontal tail, and vertical tail and threat to flight safety, were conducted rarely.

Indeed, the rotor wake is also the key factor in studying the accurate helicopter flight dynamics model. The mathematical representation of the wake generated by the rotor (viz. rotor free vortex system model) can be done in variety of way, such as by means of constant vorticity straight-line filaments, curved vortex filaments, or vortex blobs [7]. The straight-line segment approximation approach is most often used because the induced velocity contribution to each segment can be evaluated exactly using the Biot-Savart law, and involves no approximate treatment. Bagai and Leishman [8] developed a pseudo-implicit predictor-corrector (PIPC) method for the solution of the rotor free wake problem early in 1995. Since 2000, a rotor wake model based on the free vortex method has been incorporated into the helicopter flight dynamics model for the high performance helicopter design. Spoldi [9] and Horn [10] embedded the CHARM rotor free wake model [11] into the GENHEL helicopter dynamics model. Ribera [12] incorporated the free vortex model to the FLEXUM model [13].

This paper presents a mathematical model of helicopter for rotor icing analyses, by incorporating the free-wake method into the helicopter flight dynamics model. First, the methodology for the free-wake method, rotor discrete aerodynamics model, rotor ice accretion model and helicopter dynamics model was depicted. Then both the validation of the rotor wake model and effects of inflight icing on the rotor wake geometry were investigated. At last, a summary and conclusions are presented.

2. Methodology

2.1 Free-wake method

Free-wake method was developed to predict rotor wake in icing conditions, based on lifting surface theory and vortex method. The circulation of blade-attached vortex is calculated by using the lifting surface theory, and the lifting surface is arranged in the blade mid-arc surface. Along the blade-spanwise direction, the lifting surface is divided into N_r parts; in the blade-chordwise direction, it is divided into N_c parts. The entire lifting surface is divided into $N_r \times N_\mathrm{c}$ vortex lattice.

The rotor wake can be classified as near wake and far wake. The near wake is fixed in the tangent plane, which is located at the trailing edge of the blade mid-arc surface. In this region, the tip vortex is in the process of rolling up, while the inner vortex sheet is modeled in the form of quadrilateral lattice. The vortex sheet can be divided into $N_r \times N_\mathrm{w}$ vortex lattice, with N_r stations along blade-spanwise direction for each of N_w azimuthal sectors. According to the Kutta Condition [14], the circulation of each vortex lattice on the blade trailing edge at the azimuth of ψ is equal to the value of the corresponding vortex lattice circulation on the blade trailing edge at the azimuth of $\psi - \Delta\psi$, where $\Delta\psi$ is the azimuthal increment. In the far wake region, blade tip vortices roll up, forming a dominant vortex filament with high swirl velocities and relatively small viscous core, whose circulation can be taken as the peak amount of blade-attached vortex. The vortex filament of each blade can be divided into N_fw vorticity straight-line segments, and will move freely as material lines per Helmholtz's second law. Its governing equation can be written as

$$\frac{\partial \boldsymbol{r}}{\partial \psi} + \frac{\partial \boldsymbol{r}}{\partial \xi} = \frac{1}{\Omega}\boldsymbol{V} = \frac{1}{\Omega}(\boldsymbol{u}_\infty + \boldsymbol{u}_\mathrm{fw}^\mathrm{bb} + \boldsymbol{u}_\mathrm{fw}^\mathrm{b} + \boldsymbol{u}_\mathrm{fw}^\mathrm{w} + \boldsymbol{u}_\mathrm{fw}^\mathrm{fw}) \tag{1}$$

where $\boldsymbol{r}$ is the position vector of the vortex filaments, $\boldsymbol{V}$ the vector of the vortex filaments velocity, ψ and ξ the respective blade azimuth and vortex age angle, $\boldsymbol{u}_\infty$ the free stream velocity, $\boldsymbol{u}_\mathrm{fw}^\mathrm{bb}$ the velocity due to the blade motion ,and $\boldsymbol{u}_\mathrm{fw}^\mathrm{b}$, $\boldsymbol{u}_\mathrm{fw}^\mathrm{w}$, and $\boldsymbol{u}_\mathrm{fw}^\mathrm{fw}$ the velocities induced by the blade-attached vortices, the near wake vortex lattices and the far wake vortex filaments, respectively. The governing equation is solved using PIPC method. Figure 1 is the sample of the convergent rotor wake of UH-60A helicopter in hovering ($N_r = 20$, $N_\mathrm{c} = 4$, $N_\mathrm{w} = 3$, $N_\mathrm{fw} = 144$).

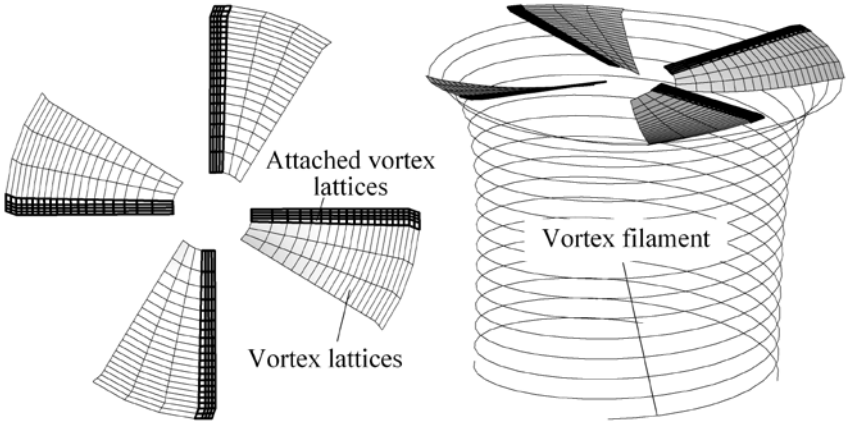

Figure 1 – Sketch of the rotor wake and its main components in hovering (i.e. the attached vortex lattices on the blades, the vortex lattices in the near wake and the vortex filament in the far wake).

2.2 Rotor discrete aerodynamic model

The rotor discrete aerodynamics model was developed as a platform to embed the free-wake model into the helicopter flight dynamics model. In the process of modelling, rotor disk was divided into $N_r \times N_\psi$ calculating sectors, with N_r stations for each of N_ψ azimuthal sectors. Thus, the discrete expressions of rotor thrust (C_T), horizontal force (C_H), side-force (C_Y), and torque (C_Q) coefficients can be deduced as

$$\begin{pmatrix} C_{\mathrm{T}} \\ C_{\mathrm{H}} \\ C_{\mathrm{Y}} \\ C_{\mathrm{Q}} \end{pmatrix} = \frac{\sigma\Delta\psi}{4\pi}\sum_{i=1}^{N_r}\sum_{j=1}^{N_\psi}\begin{pmatrix} F_c^{(i,j)}\cos\beta^{(j)} \\ F_s^{(i,j)}\sin\psi^{(j)} - F_c^{(i,j)}\sin\beta^{(j)}\cos\psi^{(j)} \\ -F_s^{(i,j)}\cos\psi^{(j)} - F_c^{(i,j)}\sin\beta^{(j)}\sin\psi^{(j)} \\ -F_s^{(i,j)}(\bar{r}^{(i)}\cos\beta^{(j)} + \bar{e}) \end{pmatrix} \tag{2}$$

where

$$F_c^{(i,j)} = (C_l^{(i,j)}\cos\beta_*^{(i,j)} - C_d^{(i,j)}\sin\beta_*^{(i,j)})F_0^{(i,j)} \tag{3}$$

$$F_s^{(i,j)} = (C_l^{(i,j)}\sin\beta_*^{(i,j)} + C_d^{(i,j)}\cos\beta_*^{(i,j)})F_0^{(i,j)} \tag{4}$$

$$F_0^{(i,j)} = \left[(\bar{u}_{\mathrm{T}}^{(i,j)})^2 + (\bar{u}_{\mathrm{P}}^{(i,j)})^2\right]\Delta\bar{r}^{(i)} \tag{5}$$

where β is the rotor blade flapping angle, β_* the blade section inflow angle, $\bar{e}$ the blade flapping hinge offset, σ the rotor solidity, and C_l and C_d the respective lift and drag coefficients of the rotor blade airfoil, and $\bar{u}_{\mathrm{T}}$ and $\bar{u}_{\mathrm{P}}$ the respective relative wind velocity and upward flapping at the blade section.

The equations of the rotor flapping coefficients (a_0, a_{1c}, a_{1s}) can be written as follows:

$$\begin{cases} f_1(a_0, a_{1c}, a_{1s}) = I_{\mathrm{b}}\Omega^2 a_0 - M_{\mathrm{T0}} + M_{\mathrm{s}}g = 0 \\ f_2(a_0, a_{1c}, a_{1s}) = M_{\mathrm{Tc}} + 2P_{\mathrm{R}}\Omega I_{\mathrm{b}} = 0 \\ f_3(a_0, a_{1c}, a_{1s}) = M_{\mathrm{Ts}} - 2Q_{\mathrm{R}}\Omega I_{\mathrm{b}} = 0 \end{cases} \tag{6}$$

where I_{b} is the rotational inertia of the blade, M_{s} the mass, g the gravitational acceleration, Ω the rotor rotational speed, and P_{R} and Q_{R} the respective rotor roll and pitch angular velocities. The expressions of M_{T0}, M_{Tc} and M_{Ts} are

$$M_{\mathrm{T0}} = \frac{\Delta\psi}{4\pi}\rho c(\Omega R)^2 R^2\sum_{i=1}^{N_r}\sum_{j=1}^{N_\psi}F_c^{(i,j)}\bar{r}^{(i)} \tag{7}$$

$$M_{\mathrm{Tc}} = \frac{\Delta\psi}{2\pi}\rho c(\Omega R)^2 R^2\sum_{i=1}^{N_r}\sum_{j=1}^{N_\psi}F_c^{(i,j)}\bar{r}^{(i)}\cos\psi^{(j)} \tag{8}$$

$$M_{\mathrm{Ts}} = \frac{\Delta\psi}{2\pi}\rho c(\Omega R)^2 R^2\sum_{i=1}^{N_r}\sum_{j=1}^{N_\psi}F_c^{(i,j)}\bar{r}^{(i)}\sin\psi^{(j)} \tag{9}$$

where ρ is the air density, c the blade chord, R the rotor radius, and $\bar{r}$ the non-dimensional local radial position along the rotor blade.

2.3 Cross coupling iteration (CCI) algorithm

In order to compute the non-uniform distribution of the rotor induced velocities and the corresponding flapping coefficients in the helicopter flight dynamics model with the free-wake method embedded a Cross-Coupling-Iteration (CCI) algorithm is proposed. Two constraints, i.e. constraint on the induced velocities iteration and constraint on the flapping coefficients iteration, are performed: 1) when the iterative numerical solution to the non-uniform distribution of the rotor-induced velocity is approaching to divergence the uniform distribution of the rotor-induced velocity based on Rotor Momentum Model (RMM) [15] can be used to as the iteration values at the moment, in order to conduct the next iteration; 2) when the rotor flapping coefficients iteration is not convergent the flapping coefficients, based on RMM, can be used to as the iteration values at the moment, in order to enter the next iteration. Figure 2 shows the flowchart of the CCI algorithm.

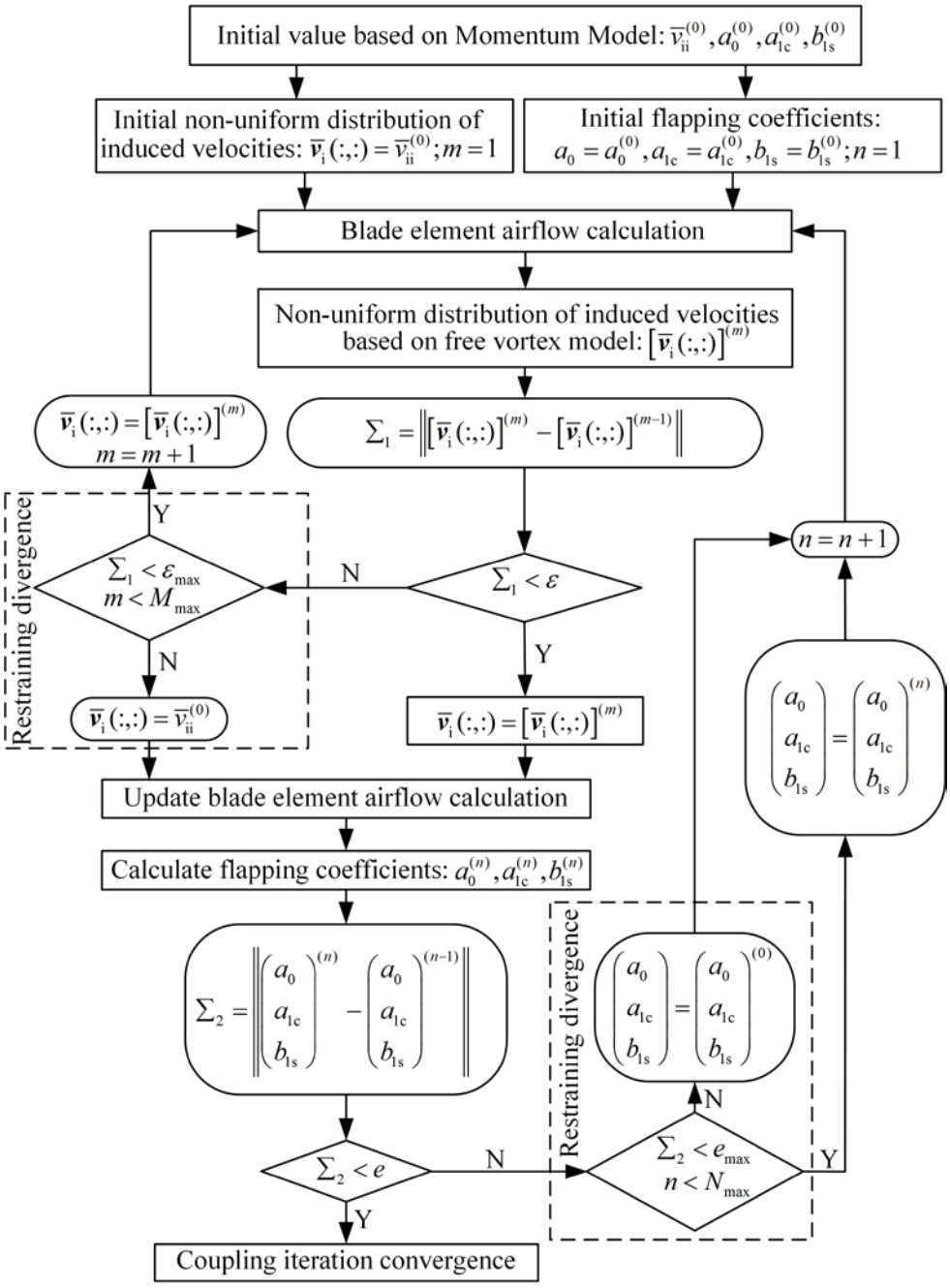

Figure 2 – Flowchart of the Cross Coupling iteration (CCI) between the induced velocities and the flapping coefficients.

2.4 Rotor ice accretion model

In order to consider the rotor ice accretion in the process of modelling, an engineering rotor ice accretion model that involves introducing the icing-related increments of rotor thrust, horizontal force, side force, torque coefficients, and icing-related increment of flapping coefficients into the uniced flight dynamics model was developed [4]. The basic lift and drag coefficients of the rotor-blade airfoil due to icing can be written in the form

$$\begin{cases} C_L' = (1 + \Delta C_L / C_L) C_L \\ C_D' = (1 + \Delta C_D / C_D) C_D \end{cases} \tag{10}$$

where C_L', C_L and ΔC_L are the respective iced, clean and incremental lift coefficients of the rotor-blade airfoil, and C_D', C_D and ΔC_D the respective iced, clean and incremental drag coefficients of the rotor-blade airfoil. Coefficients of rotor thrust, side force, horizontal force, torque, and flapping coefficients due to icing can be written as the same forms.

2.5 Flight dynamics model

By combining with the free-wake method, the rotor discrete aerodynamics model, the CCI algorithm and the rotor ice accretion model, a helicopter dynamics model in icing conditions can be developed. First, the initial helicopter dynamics trim calculation can be conducted based on the Rotor Vortex Model (RVM) [15]. Following this, the iteration of the rotor free wake can be conducted by using PIPC algorithm in order to solve the convergent wake geometry based on the corresponding helicopter dynamics trim results. Using the convergent rotor wake calculated by the free vortex wake model, the non-uniform distribution of the rotor-induced velocity can be calculated. Later the rotor ice accretion model is integrated into the rotor discrete aerodynamics model, which allows the model to predict the increments of iced rotor force and torque and rotor flapping coefficients. Thus the free-wake method incorporation into the helicopter flight dynamics model in icing conditions can be realized. Figure 3 shows the flow chart of implementing the helicopter dynamics trim in icing conditions.

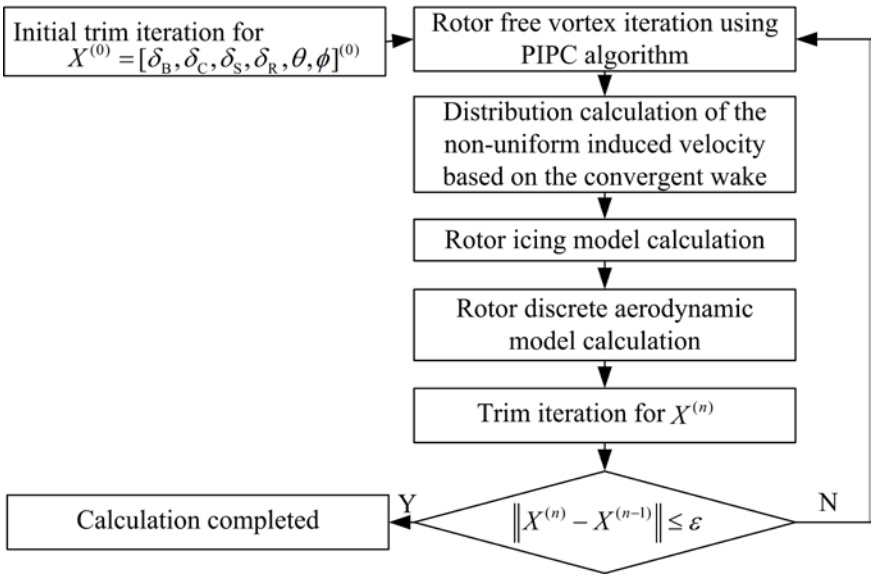

Figure 3 – Flowchart of implementing the helicopter trims in icing conditions.

3. Validation

3.1 Validation of the free-wake method

Validity and accuracy of the free-wake method are verified through comparison with the available experimental measurements [16]. The model rotor geometry and the operating conditions for the rotor configuration are summarized in Table 1. Figure.4 shows the free wake predictions along with the experimental measurements.

It can be indicated that the predictions and measurements are in good agreement with the exception of some discrepancies in the wake age from 0 to 180deg. The reason for the discrepancies can be drawn as that the release point position of each blade tip vortex in the model is set at the end of the row of the vortex lattice in the near wake that is fixed on the tangent plane of the trailing edge of the blade middle curve surface, thus the vertical position of the vortex lattices in the near wake are fixed and the vertical position of the tip vortex in the wake age from 0 deg to180 deg are fixed.

Table 1 – Operating conditions for the rotor configuration.

Blade number	1
Radius, m	0.4064
Chord, m	0.0425
Hinge offset, $\bar{e}$	0.0
Spar length, $\bar{r}_0$	0.2
Tip speed, m/sec	89.37
Airfoil section	NACA2415
Collective pitch, deg	4.0
Twist, deg	0.0
Thrust coefficient	0.003

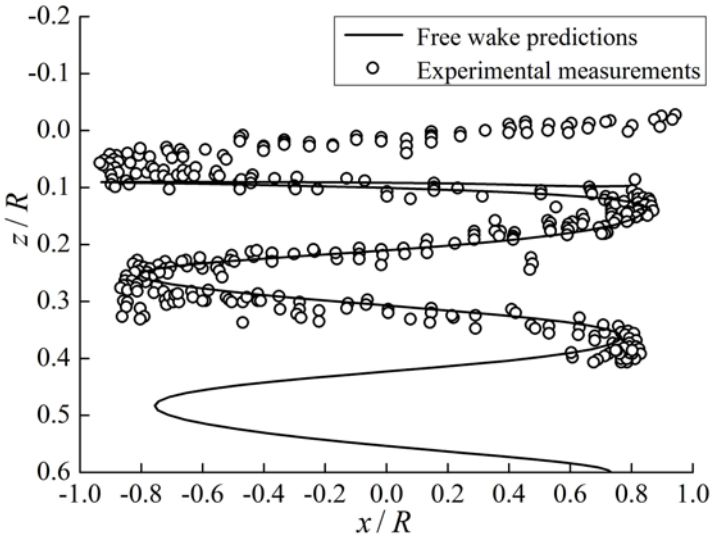

Figure 4 – Free wake predictions along with the experimental measurements.

Figure 5 shows the convergent rotor wake geometries of UH-60A helicopter at the different flight velocities in the clean ice condition. It can be shown that the free-wake method embedded in the helicopter flight dynamics model can well capture the rotor wake geometric characteristics. With the increase in flight velocity, the process of the tip vortex rolling up of rotor blade is also well demonstrated.

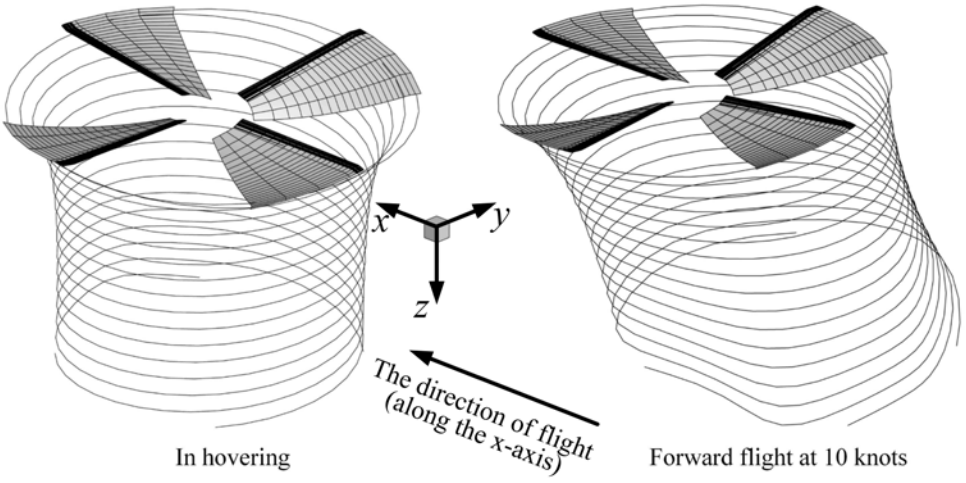

(a)

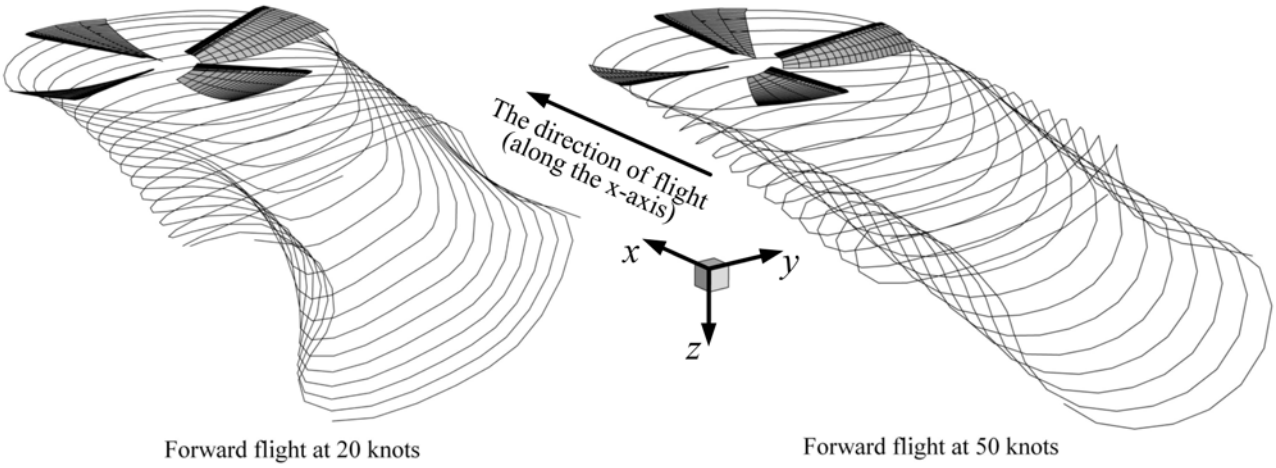

(b)

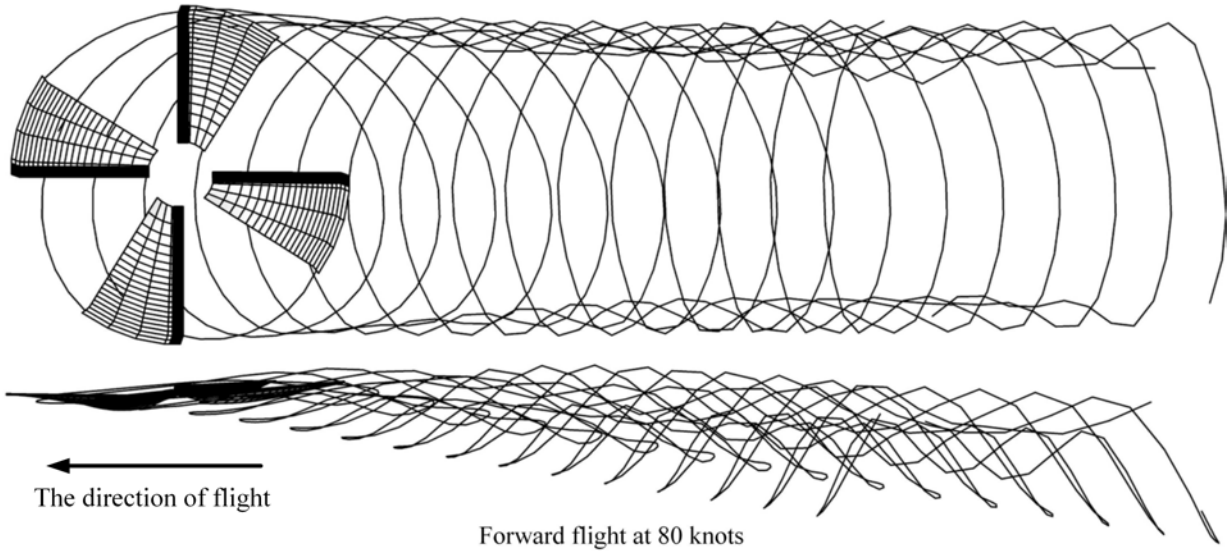

(c)

Figure 5 – The rotor wake geometries of UH-60A helicopter at different flight velocities: (a) 0knots and 10knots, (b) 20knots and 50knots and (c) 80knots.

3.2 Validation of the rotor ice accretion model

To validate the rotor ice accretion model, the iced lift and drag coefficients of the rotor blade airfoil of UH-60A helicopter are computed and compared with the icing wind tunnel test data [17], as shown in Figure 6. The airfoil operates on Mach number of about 0.6 and the angle of attack of about 6 degrees in the icing conditions (i.e. the liquid water content is 0.66g/m^3, the median volumetric diameter of the cold water drop is 20μm, and the icing time is 45 s). It can be shown that the rotor icing model is fidelity and effective because the results match well with the test data. In addition, it can be also found that ice accretion on the blade airfoil decreases the lift coefficient and increases the drag coefficient, and that as the increase in the atmospheric temperature (from about -30 degree Celsius to about -10 degree Celsius) in icing conditions, the lift coefficient will continue to decrease and the drag coefficient will continue to increase. The reason for this is that different ice shapes on the airfoil have different effect on the aerodynamics. In detail, the adverse effect of the rime ice accreted in a lower atmospheric temperature on the aerodynamics is better than that of mixed ice and glaze ice accreted in a higher atmospheric temperature, though all these aerodynamics performance are degraded evidently. Detailed analyses on the distribution of the ice shapes on the blades of the rotor disk will be illustrated in sec.4.

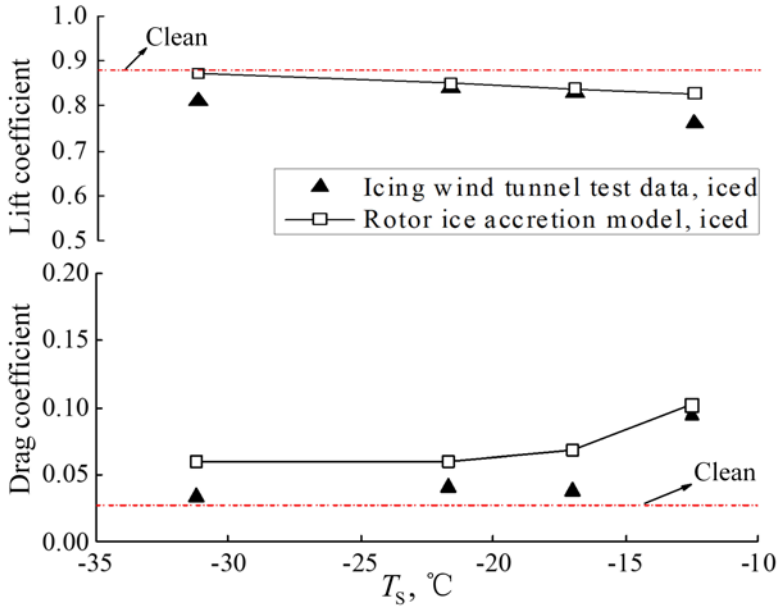

Figure 6 – The iced lift and drag coefficients of SC 1095 airfoil along with the wind tunnel test data.

4. Analyses

In this paper, the basic icing conditions mainly consist of atmospheric temperature (T_S), liquid water content (*LWC*), median volumetric diameter (*MVD*) of the cold water drop and icing time (τ) which are shown in Table 2. Effects of icing time (τ) and atmospheric temperature (T_S) on the rotor wake are primarily analyzed. Note that the wake of one blade at the azimuth of zero degree is shown and analyzed in detail for the sake of convenience.

Table 2 – Basic icing conditions.

T_S, ℃	*LWC*, g/m^3	*MVD*, μm	τ, sec
-26.0	1.0	20.0	180.0

4.1 Rotor wake geometry due to icing time

Figure 7 gives the effects of icing on the rotor wake due to icing time in hovering. In Figure 7, rotor icing makes the wake geometry slightly sink. This also induces the wake geometry to slightly move along the azimuth of 180 and 90 degrees. And as the icing time increases, the variation trend become increasing obvious. Furthermore, Figure 7 presents the heights of the blade tip vortex filament versus vortex age angle (ξ) and the specific changes in the sunk amplitude of the wake.

Some reasons for the rotor wake changes with icing time might be due to the effects of icing on the angle of attack (AOA) of the rotor blade. In comparing the uniced distribution of AOA, Figure 8 gives the effects of icing on the distribution of AOA due to icing time, which ranged from 180 s to 300 s, and to 360 s. It can be indicated that the AOA of the rotor blade increases with icing time. Furthermore, the AOAs of the rotor blade exhibit an evident increase with icing time at both the blade tip area of the front-half part and the blade root area of the back-half part of the rotor disk.

The wake sinks and increased AOAs due to ice accretion would make the rotor blade lift increase according to the principles of aerodynamics. This seems to be conflict with the surely proven fact (i.e. the airfoils of the rotor blade experience a lower lift coefficient in icing conditions). This is not the case, however, as the helicopter is inflight thus it needs to maintain a stable flight state by at least increasing the collective pitch so as to increase the AOA and generate more lift and thus make the wake sink. This is actually the intuitive reason for the sinking of the wake when flying in icing conditions.

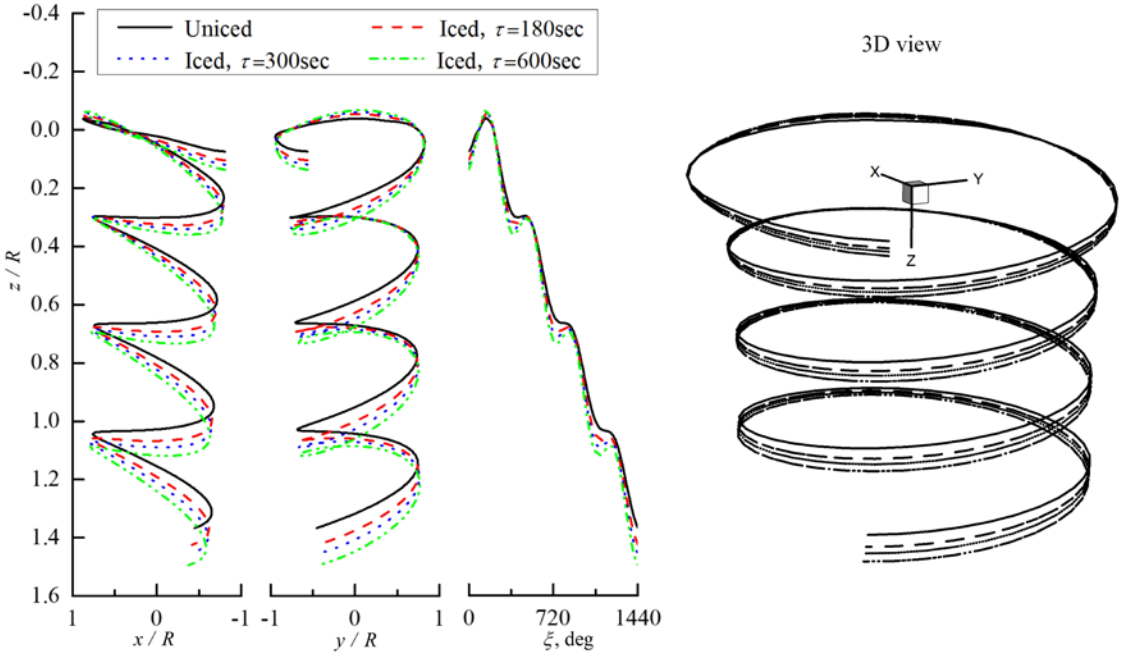

Figure 7 – Effects of icing on the rotor wake due to icing time (τ) in hovering.

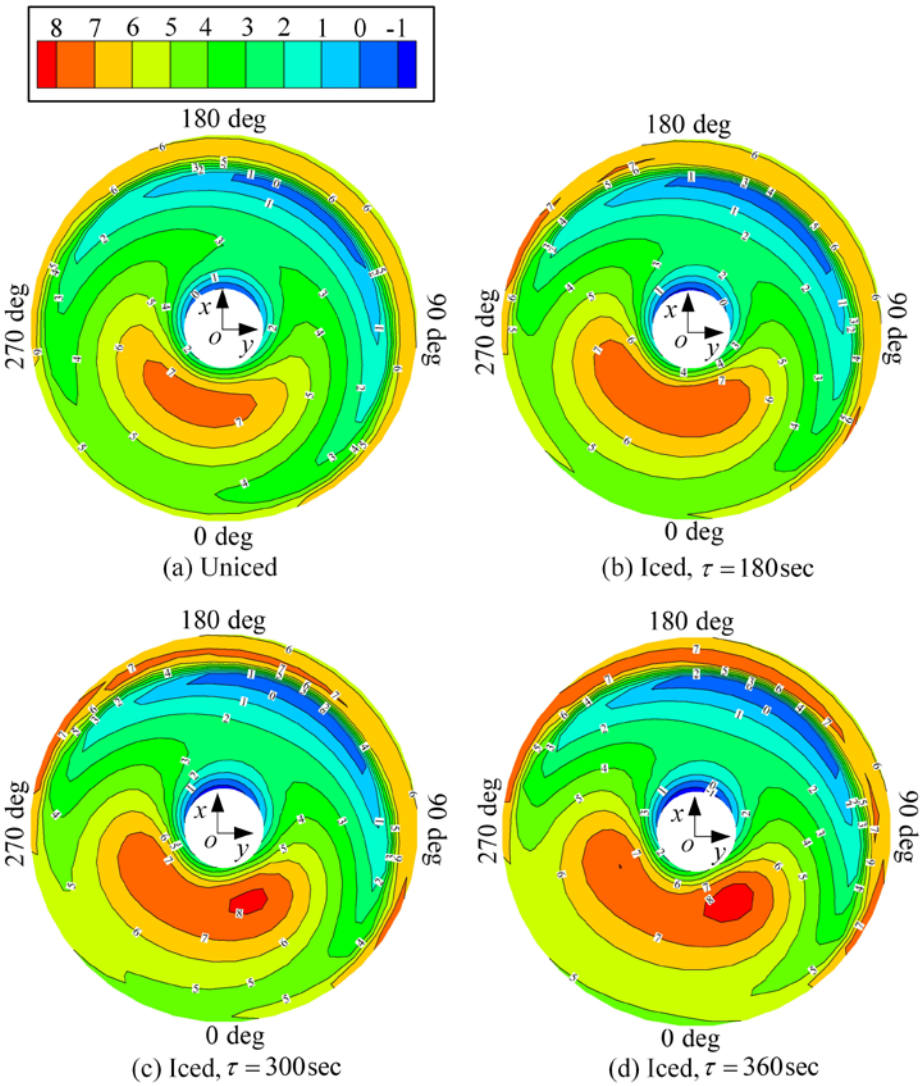

Figure 8 – Effects of icing on the AOA of the rotor blade due to icing time (τ) in hovering.

4.2 Rotor wake geometry due to atmospheric temperature

Figure 9 gives the effects of icing on the rotor wake due to atmospheric temperature (T_S) in hovering. In Figure 9, rotor icing makes the wake slightly sinks when the atmospheric temperature degrades from -12 degree Celsius to -20 degree Celsius. However, this causes the sunk trend to slightly recover when the atmospheric temperature continues to degrade from -20 degree Celsius to -26 degree Celsius. Figure 9 indicates the heights of the blade tip vortex filament versus vortex age angle (ξ), and the specific changes in amplitude of this trend.

Some reasons for this change trend might be due to the temperature effects. Generally, the performance penalty caused by glaze ice is more serious than that by mixed ice and subsequently rime ice. The rotor icing tunnel test data indicates that as the temperature increased, the accreted ice shape on the outer portion of the rotor blades changed from rime to mixed and subsequently to glaze, increasing the performance penalties [2]. In this section, the distribution of the ice shape on the rotor disk at different atmospheric temperatures was calculated to validate the change trend of the effects of icing on rotor wake due to atmospheric temperature by using the ice shape definition method [4], as shown in Figure 10.

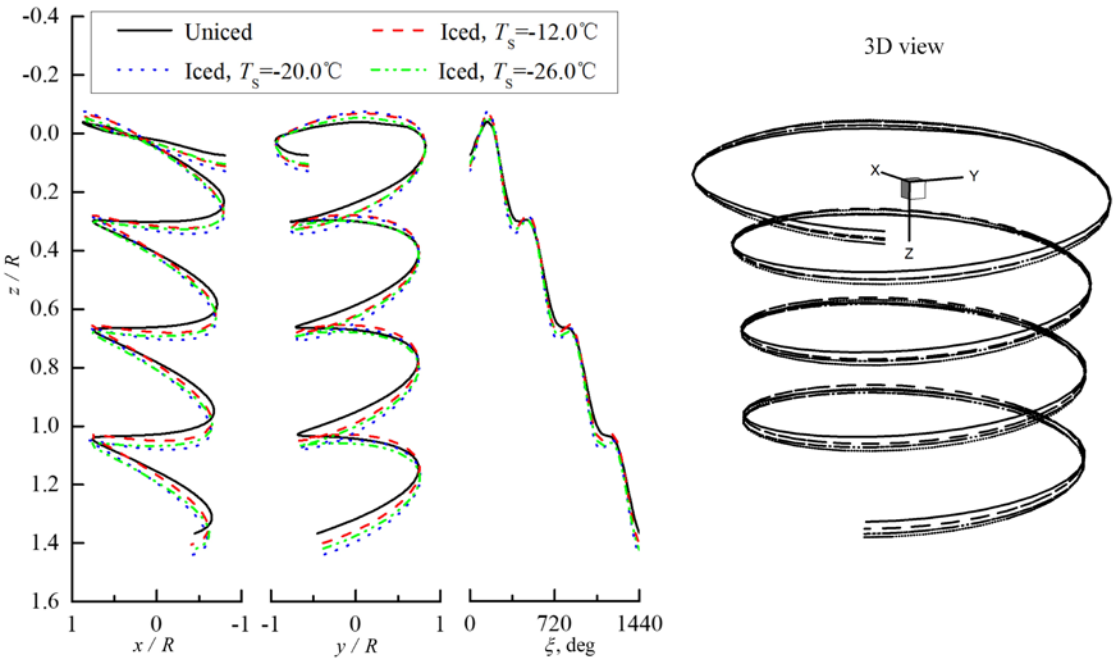

Figure 9 – Effects of icing on rotor wake due to atmospheric temperature (T_S) in hovering.

In Figure 10, it can be observed that the range of the glaze ice accreted on the outer portion of the rotor blades significantly increases when the atmospheric temperature degrades from -12 degree Celsius to -20 degree Celsius, increasing the performance penalties, and subsequently making the rotor wake sink (see Figure 9). However, the range of the rime ice accreted on the inner portion of the rotor blades evidently increases when the atmospheric temperature degrades from -20 degree Celsius to -26 degree Celsius, decreasing the performance penalties and making the rotor wake have a slightly reverted change trend to the uniced state (see Figure 9). The reason for this is that the performance penalty due to rime ice is lower than the glaze ice, and that this has an irregular shape. In addition, the uniced area on the blade tip region in Figure 10 is generated by an extremely high local temperature, preventing the occurrence of ice accretion. The reason for this is that there might be a positive correlation between the high local temperature and the high local Mach number at the blade tip region.

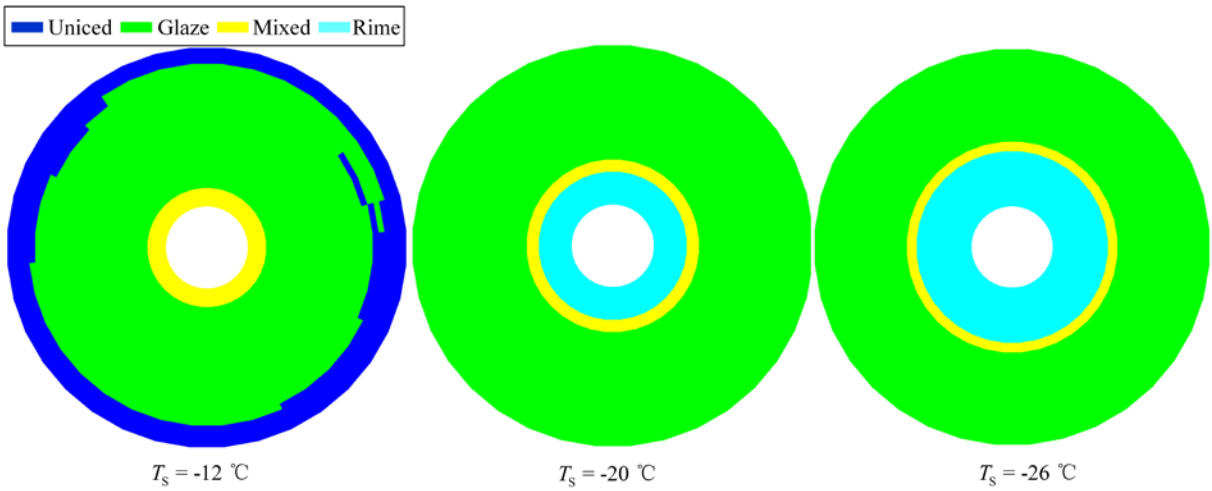

Figure 10 – The distribution of the ice shape on the blades of the rotor disk in hovering.

5. Conclusions

A helicopter flight dynamics model with free-wake method embedded for rotor icing analysis is established in order to acquire the convergent rotor wake geometries and to investigate the effects of inflight icing on those wake geometries. This proposed methodology appears to be an adequate tool for rotor icing analyses.

Our results indicate that both the sunk trend of the rotor wake due to icing and the variation of ice

shape on the rotor blades might lead to the rotor aerodynamics performance degradation. On the one hand, the ice accretion makes rotor wake sink. The sunk trend becomes more evident with the increase in icing time. On the other hand, the rime-ice shape firstly occurs on the inner portion of the rotor blades. It diffuses outward along the blade with the decrease in atmospheric temperature. In addition, the uniced area of the rotor blade tip is generated by the so high local temperature that the ice accretion does not occur, but the glaze-ice shape occurs when the atmospheric temperature continues to lower.

6. Contact Author Email Address

liguozhi20@163.com

7. Copyright Statement

References

[1] Korkan K, Dadone L and Shaw R. Helicopter rotor performance degradation in natural icing encounter. *Journal of Aircraft*, Vol. 21, No. 1, pp 84-85, 1984.

[2] Flemming R, Randall K and Thomas H. Role of wind tunnels and computer codes in the certification and qualification of rotorcraft for flight in forecast icing. NASA TM-106747, 1994.

[3] Cao Y H, Li G Z and Zhong G. Tandem helicopter trim and flight characteristics in the icing condition. *Journal of Aircraft*, Vol. 47, No. 5, pp 1559-1569, 2010.

[4] Cao Y H, Li G Z and Hess R. Helicopter flight characteristics in icing conditions. *The Aeronautical Journal*, Vol. 116, No. 1182, pp 963-979, 2012.

[5] Cao Y H, Wu Z L and Su Y. Aircraft flight characteristics in icing conditions. *Progress in Aerospace Sciences*, Vol. 74, pp 62-80, 2015.

[6] Cao Y H, Tan W Y and Wu Z L. Aircraft icing: An ongoing threat to aviation safety. *Aerospace Science and Technology*, Vol. 75, pp 353-385, 2018.

[7] Leishman J. *Principles of helicopter aerodynamics*. Cambridge University Press, 2000.

[8] Bagai A, Leishman J. Rotor free-wake modeling using a pseudo-implicit technique – including comparisons with experimental Data, *Journal of American Helicopter Society*, Vol. 40, No. 3, pp 29-41, 1995.

[9] Spoldi S, Ruckel P. High fidelity helicopter simulation using free wake, lifting line tail, and blade element tail rotor models. *59th Annual Forum of AHS*, Phoenix AZ, 2003.

[10] Horn J, Bridges D and Wachspress D. Implementation of a free vortex wake model in real time simulation of rotorcraft, *61th Annual Forum of AHS*, Grapevine TX, 2005.

[11] Wachspress D, Quackenbush T and Boschitsch A. First-principles free vortex wake analysis for helicopter and tilt-rotors, *59th Annual Forum of AHS*, Phoenix AZ, 2003.

[12] Ribera M. *Helicopter flight dynamics simulation with a time accurate free vortex wake model*. University of Maryland, 2007.

[13] Kim F, Celi R and Tischler M. High-order state space simulation models of helicopter flight mechanics, *Journal of the American Helicopter Society*, Vol. 38, No. 4, pp 16-27, 1993.

[14] Katz J, Plotkin A. *Low-speed aerodynamics*. Cambridge University Press, 2001.

[15] Cao Y H, Li G Z and Yang Q. Studies of trims, stability, controllability, and some flying qualities of a tandem rotor helicopter, *Proceedings of the Institution of Mechanical Engineers, Part G: Journal of Aerospace Engineering*, Vol. 223, No. (G2), pp 171-177, 2009.

[16] Bhagwat M. *Mathematical modeling of the transient dynamics of helicopter rotor wakes using a time accurate free vortex methods*. University of Maryland, 2001.

[17] Flemming R and Lednicer D. High Speed Ice Accretion on Rotorcraft Airfoils. NASA CR 3910, 1985.